Immune engineered extracellular vesicles to modulate T cell activation in the context of type 1 diabetes

Matthew W. Becker[1], Leeana D. Peters[2,3], Thinzar Myint[2,3], Dylan Smurlick[1], Andrece Powell[1], Todd M. Brusko[2,3,4], Edward A. Phelps[1,2,3*]

[1] J. Crayton Pruitt Family Department of Biomedical Engineering, University of Florida, Gainesville, FL.

[2] Department of Pathology, Immunology, and Laboratory Medicine, College of Medicine, University of Florida, Gainesville, FL.

[3] University of Florida Diabetes Institute, University of Florida, Gainesville, FL.

[4] Department of Pediatrics, College of Medicine, University of Florida, Gainesville, FL.

[*] correspondence: ephelps@bme.ufl.edu

Abstract

Extracellular vesicles (EVs) are small, biologically active, cell-secreted vesicles that can affect immune responses through antigen presentation and co-stimulation or co-inhibition. We generated designer EVs to modulate autoreactive T cells in the context of type 1 diabetes (T1D) by engineering a lymphoblast cell line, K562, to express HLA-A*02 (HLA-A2) alongside co-stimulatory CD80 and/or co-inhibitory PD-L1. T1D is an autoimmune disease primarily mediated by T cells that selectively destroy insulin-producing beta cells, and inhibiting tissue-specific T cells is a promising strategy for treating T1D. EVs presenting HLA-A2 and CD80 activated $CD8^+$ T cells in a dose, antigen, and HLA-specific manner. Adding PD-L1 to these EVs produced an immunoregulatory response, reducing $CD8^+$ T cell activation and cytotoxicity *in vitro*. EVs alone could not stimulate T cells without antigen presenting cells (APCs), suggesting that EVs act by cross-dressing APCs. EVs lacking CD80 were ineffective at modulating $CD8^+$ T cell activation, suggesting that both peptide-HLA complex and costimulatory molecules are required for EV-mediated immune modulation through APC cross-dressing. These results provide mechanistic insight into the rational design of EVs as a cell-free, yet precision medicine-based approach to immunotherapy that can be tailored to promote antigen-specific immune tolerance or pro-inflammatory responses.

Keywords

Extracellular vesicles, immune engineering, PD-L1, CD80, type 1 diabetes

Introduction

Extracellular vesicles (EVs) are small, biologically active vesicles secreted by most cell types that either derive from the endocytic compartment or are shed from the cell membrane (*1*). Small EVs (30-150 nm), which are often referred to as exosomes (*2, 3*), play important roles as messengers carrying information through proteins, nucleic acids, lipids, and metabolites that exert effects on interacting cells (*4-7*). EV membranes contain lipid rafts that are enriched in cholesterol, sphingomyelin, and ceramide, making them highly stable in body fluids (*8*) and thus, an attractive tool for therapeutics. Furthermore, EVs are a source of peptide-MHC (pMHC) and can interact with the immune system in multiple ways in an antigen-specific manner (*9*). Given these advantages, EVs present an attractive modular tool for novel therapeutic development and can be altered in many cases to complement or enhance their potential therapeutic applicability (*10-13*).

Our approach to EV engineering is inspired by the role of endogenous EVs in disease settings such as cancer or autoimmunity (*14, 15*). For example, tumor cell exosome-presented programmed death-ligand 1 (PD-L1) regulates T cell responses in cancer (*16, 17*). Binding of PD-L1 to its receptor PD-1 on T cells results in strong countering of T cell receptor (TCR) signal transduction and CD28 co-stimulation (*18, 19*), thereby suppressing antigen driven activation of T cells. Removal of PD-L1 specifically from exosomes leads to strong T cell activation and tumor rejection (*20*). In autoimmunity, EVs have been shown to potentially contribute to disease progression through immune activation. For example, in type 1 diabetes (T1D), islet autoantigens such as insulin, glutamic acid decarboxylase 65 (GAD65), and insulinoma-associated protein-2 (IA-2) have been identified in beta cell EVs, which can then be transferred to antigen presenting cells (APCs) for processing and presentation to T cells (*21-23*). This route of beta cell autoantigens becoming available to the immune system may play a role in the initiation and progression of T1D. Many dysregulated immune pathways in cancer and autoimmunity may be modulated, at least in part, by contributions from EVs (*14, 15*). Determining the mechanisms by which EVs impart these effects may provide insights into how to effectively engineer and leverage them in an *ex vivo* setting for therapeutic purposes.

Here, we investigated the negative regulatory properties of engineered EVs as a tool for modulating T cell activation and cytotoxicity to combat the autoimmune component of T1D. HLA molecules present antigenic peptides to T cells for immune surveillance, and it is well documented that certain combinations of HLA alleles confer genetic risk or protection from T1D (*24*). We designed an *in vitro* system for generating and testing EVs carrying autoantigen-loaded HLA class I molecules using the T1D risk-associated HLA-A*02, plus co-stimulation with or without PD-L1 co-inhibition. We demonstrated the importance of APCs in EV-mediated activation of $CD8^+$ T cells, as well as a potential role for CD80 in both EV-mediated stimulation and inhibition. We also

generated islet-autoreactive human $CD8^+$ T cell "avatars" and showed that immune engineered EVs reduced T cell-mediated killing of target cells *in vitro*. Our results provide valuable insight into effective EV engineering with applications for tissue-specific immune modulation.

Results

EV isolation and characterization. When determining a suitable system to use for generating EVs and investigating their immunomodulatory effects, we chose to engineer an *in vitro* system with relevance to T1D. Insulin is one of the primary autoantigens in T1D (*25*), with several pre-proinsulin peptides inducing $CD8^+$ T cell mediated autoimmunity through HLA-A*02 presentation (*26*). K562 cells are a lymphoblast cell line widely used as an artificial antigen presenting cell (aAPCs) due to their lack of classical HLA I and II molecules combined with their amenability to genetic manipulation (*27*). K562 cells modified to express CD80, CD83, HLA-A*02 and pre-proinsulin (K562 A2/PPI) were used as aAPCs and were the cell source for generating EVs (Supplemental Figure 1). THP-1 cells, which are a monocytic cell line that expresses HLA-A*02 but not CD80 (Supplementary Figure 2A), were also used for generating EVs.

While ultracentrifugation has been a common method for small EV isolation (*28*), this can lead to vesicle damage and aggregation (*29, 30*). One alternative method that avoids this potential limitation uses liquid chromatography columns for bind-elute size exclusion chromatography separation (BE-SEC) of small EVs from conditioned medium (*31*). We adopted this method, in combination with ultrafiltration steps before and after chromatography separation, to isolate EVs for use in functional assays (Figure 1A). NTA of EVs from both K562 A2/PPI (K-EV) and THP-1 (T-EV) cells isolated through chromatography consistently showed a homogeneous particle size distribution, with diameters across multiple isolations between 40 and 110 nm (Figure 1B, Supplementary Figure 3A). Western blot analysis demonstrated the presence of small EV markers ALIX and Sytenin-1 (*32*) in both K-EVs and T-EVs (Figure 1C, Supplementary Figure 3B). We were also able to detect HLA-A in EVs from both cell lines (Figure 1C, Supplementary Figure 3B), indicating that HLA is trafficked to EVs from parent cells. TEM imaging of K-EVs showed particles with typical size and cup-shaped morphology (*33*) (Figure 1D). Additionally, comparing NTA data across multiple EV batches isolated through BE-SEC showed a consistent batch-to-batch particle size of 42-75 nm (Supplementary Figure 4A). UV chromatograms from BE-SEC isolations showed good peak separation of EVs from soluble proteins and were consistent between batches of different starting volumes (Supplementary Figure 4B). Western blot analysis showed the presence of the canonical EV marker ALIX in EVs isolated through both BE-SEC and ultracentrifugation (Supplementary Figure 4C), but NTA data across multiple EV batches isolated through ultracentrifugation showed wider batch-to-batch variability and less consistent particle

size distributions compared to BE-SEC preps (Supplementary Figure 4D). These data together demonstrate that K562 A2/PPI cells and THP-1 monocytes secrete small EVs, which we can purify from conditioned medium in a scalable and reproducible manner.

Validating an in vitro target:effector co-culture model for EV engineering. Prior to investigating the immunomodulatory effects of EVs, we first validated that K562 A2/PPI aAPCs, the cells used for manufacturing K-EVs, could activate cognate T cells *in vitro*. Jurkat T cells were engineered as model effector cells to express CD8 and the 1E6 TCR (hereafter referred to as J-1E6 T cells), which recognizes PPI_{15-24} presented in HLA-A*02 (*34*). To validate that K562 A2/PPI cells could activate J-1E6 cells, we performed co-cultures using IL-2 secretion as a readout of T cell antigen recognition and activation (*20*). K562 cells devoid of any modifications (K562 HLA null) were used as negative controls to ensure that T cell IL-2 secretion was dependent on HLA-presented peptide (Figure 2A). T cells did not secrete any IL-2 when co-cultured with K562 HLA null cells even with addition of exogenous PPI_{15-24} peptide, or when cultured with exogenous peptide in the absence of K562 cells (Figure 2B). Conversely, T cells cultured with K562 A2/PPI cells secreted IL-2, albeit to a lower extent than positive control cells activated with PMA and ionomycin (Figure 2B). Adding exogenous PPI_{15-24} peptide to co-cultures with T cells and K562 A2/PPI cells significantly increased IL-2 secretion above similar cultures without exogenous peptide addition (Figure 2B). K562 A2/PPI cells loaded with a different islet antigen peptide, $IGRP_{265-273,}$ failed to induce IL-2 secretion from T cells above control levels without exogenous PPI loading (Supplementary Figure 5). THP-1 cells, which express HLA-A*02 but not CD80, were cultured with J-1E6 cells in a similar manner with or without exogenous PPI_{15-24} peptide. THP-1 cells failed to induce IL-2 secretion from T cells even with peptide loading, indicating the necessity of CD80 co-stimulation in this model (Supplementary Figure 2B). We also performed flow cytometry to evaluate cell surface markers of activation on J-1E6 cells after 2, 4, and 24 hours of co-culture with K562 A2/PPI cells. J-1E6 T cells co-cultured with K562 A2/PPI cells expressed significantly more CD69 (Figure 2C) and PD-1 (Figure 2D) compared to T cells alone. These results indicate that J-1E6 T cells recognize and react in response to PPI_{15-24} presented in HLA-A*02 on K562 A2/PPI cells and provide a foundation for investigating the immunomodulatory effects of EVs generated from these model cells.

EVs need APCs to modulate T cell activation in vitro. Having established our EV source and *in vitro* model, we next examined the effects of EVs on T cell activation, as there is evidence showing that EVs can influence T cells through a variety of mechanisms including direct T cell contact (*35*, *36*), cross-presentation by APCs, or cross-dressing of APCs (*37*, *38*). Cross-dressing refers to the passage of EV pHLA and other molecules to an APC without further antigen

processing. We added increasing numbers of K-EVs to co-cultures with T cells and K562 A2/PPI cells (Figure 3A) and measured IL-2 secretion after 24 hours. Addition of K-EVs caused an increase in IL-2 secretion in a dose-dependent manner (Figure 3B). However, the addition of K-EVs to J-1E6 T cells in the absence of aAPCs did not result in significant IL-2 induction when compared to T cells alone (Figure 3C), even with addition of exogenous PPI_{15-24} peptide (Figure 3D). To further examine the mechanism of EV immune activity, we labeled EVs with DiR and added them to cultures with either J-1E6 T cells alone, K562 A2/PPI cells alone, or J-1E6 and K562 A2/PPI cells together (Figure 3E). Cell membranes were labeled with lipophilic dyes prior to the start of the experiment to allow for visualization, and after 24 hours of co-culture we performed confocal microscopy. Intracellular and cell surface DiR signal was detectable in K562 A2/PPI cells alone or in co-culture with T cells, but EV uptake was undetectable for J-1E6 T cells (Figure 3F). High-resolution 3D micrographs also showed evidence of EV clusters on K562 A2/PPI cell surfaces (Figure 3G). Quantification of intracellular DiR signal from EVs further confirmed that EV uptake occurred in K562 cells, but not J-1E6 T cells (Figure 3H). These results suggest that K-EVs pass their contents to K562 A2/PPI cells but do not interact directly with J-1E6 T cells. Conversely, adding T-EVs, which contain pHLA but not CD80, to co-cultures of T and K562 A2/PPI cells failed to increase IL-2 secretion (Supplementary Figure 6). This result suggests that EV CD80 is important for EV immune activity in our model, although other differences in EV protein expression between the two different parental cell lines K562 and THP-1 could also be important. Blocking CD80 interactions in the co-culture system with an antibody eliminated the IL-2 response from T cells, demonstrating the necessity for CD80 co-stimulation in our system (Supplementary Figure 7) and suggests that EVs lacking CD80 would be unlikely to contribute to T cell signaling. Taken together, these data show that T cell stimulation in our system through aAPCs alone or aAPCs with EVs, requires pHLA and co-stimulatory molecules such as CD80. Other differences in EV composition, especially when derived from different cell sources may also contribute to the overall response.

Driving PD-L1 expression in EV parent cells. EV PD-L1 incorporation correlates with cellular expression levels, as cells naturally shuttle the protein to EV membranes (*39*). We therefore reasoned that we could purify PD-L1$^+$ EVs from PD-L1 expressing cells. While many cells such as THP-1 monocytes upregulate PD-L1 expression in the presence of inflammatory cytokines like IFN-γ (*40-42*) (Supplementary Figure 8A), we chose to create a K562 A2/PPI cell line stably expressing PD-L1 through lentiviral transduction. After lentiviral transduction, we sorted and expanded PD-L1$^+$ K562 A2/PPI cells (K562 PD-L1), then confirmed stable PD-L1 expression via flow cytometry and western blot after several passages (Figure 4A). Recent work has highlighted the influence of *cis*-PD-L1/CD80 binding and its inhibitory effect on these

molecules binding in *trans* to PD-1 and CD28 or CTLA-4 (*43*, *44*). While CD80 typically exists as a homodimer in cell membranes, its affinity for PD-L1 is higher than it is for itself (*45*), which can lead to preferential formation of PD-L1/CD80 heterodimers (i.e., *cis*-PD-L1/CD80). These heterodimers block PD-L1 from binding to PD-1 on other cell membranes, thus inhibiting *trans*-PD-L1/PD-1 signaling (*44*). In particular, high CD80 expression can lead to increased *cis*-PD-L1/CD80 heterodimers and subsequent decreased *trans*-PD-L1/PD-1 binding. As such, our next step was to ensure that K562 PD-L1 cells would suppress T cell activation in our co-culture model (Figure 4B). We cultured J-1E6 T cells with K562 A2/PPI or K562 PD-L1 cells, with or without exogenous PPI_{15-24} peptide for 24 hours and measured IL-2 secretion in the supernatant. Co-culture of T cells and K562 PD-L1 cells resulted in less IL-2 production as compared to co-culture with K562 A2/PPI cells, even with exogenous peptide (Figure 4C). The results shown here indicate K562 cells presenting PD-L1 alongside cognate pHLA complexes can reduce T cell activation in our model, despite high CD80 expression on K562 aAPCs.

Validating PD-L1 expression in EVs. We next sought to characterize EVs from K562 PD-L1 cells (K-PD-L1-EV). NTA analysis of K-PD-L1-EVs showed a homogeneous size distribution with mean particle diameters similar to K-EVs (Figure 5A). Further, we detected PD-L1 in EV isolates through an ELISA (Figure 5B). We also detected PD-L1 in EVs from THP-1 cells cultured with IFN-γ (T-PD-L1-EV, Supplementary Figure 8B). These results demonstrate that stable expression of PD-L1 in parent cells naturally leads to packaging of PD-L1 into EVs, which is detectable together with HLA.

K-PD-L1-EVs suppress T cell activation. The expression of PD-L1 on EVs in circulation is associated with poor outcomes of anti-PD-1 cancer therapies (*17*) due to their ability to suppress cytotoxic T cells that would normally eradicate tumor cells. Removal of PD-L1 specifically in EVs restores anti-tumor immunity (*20*). To examine if reciprocal effects can be observed in the context of the autoimmune disease T1D, we tested EVs with PD-L1 in our *in vitro* target:effector co-culture model (Figure 6A). Increasing amounts of K-PD-L1-EVs in co-culture with T cells and K562 A2/PPI cells led to a decrease in IL-2 secretion in a dose-dependent manner (Figure 6B). Given that these co-cultures were performed with aAPCs completely devoid of PD-L1, these results show that EV PD-L1 is capable of inhibiting antigen recognition-induced activation of T cells specific for a T1D autoantigen. However, this seems to depend on the presence of CD80 on the EVs, as adding T-PD-L1-EVs without CD80 to co-cultures resulted in only a modest decrease in IL-2 secretion from J-1E6 cells that was similar in magnitude to cultures with a large dose of T-EVs (Supplementary Figure 8C).

We performed an analysis across all experiments with EV treatments and compared the fold change in IL-2 secretion (Figure 6C). EVs from K562 cells with or without PD-L1 significantly decreased and increased IL-2 secretion, respectively. EVs from THP-1 cells did not have a significant effect on IL-2 secretion. This analysis provides further evidence that regardless of HLA or PD-L1 expression in EVs, the cell source and additional co-stimulatory markers are important to impart immunomodulatory effects.

EV PD-L1 reduces T cell-mediated target cell killing in vitro. While Jurkat T cells are a suitable cell line to use for proof-of-principle studies with therapies intended to modulate T cell functionality, they are not true effector cells and thus, lack any appreciable cytotoxic capabilities. We therefore replaced J-1E6 cells with a more authentic effector T cell in our co-culture model (Figure 7A) to determine if PD-L1 presenting EVs still exert their suppressive effects, while keeping our studies within the context of T1D. Primary human $CD8^+$ T cell "avatars" were generated to express a TCR specific for the IGRP peptide $IGRP_{265\text{-}273}$ presented in HLA-A*02, which is a known autoantigen in the human T1D population (*46*) (referred to here as T-IGRP cells). K562 aAPCs (either K562 A2/PPI or K562 PD-L1) were loaded with exogenous $IGRP_{265\text{-}273}$ peptide prior to co-culture with T-IGRP cells and/or K-PD-L1-EVs to provide T cell recognition of cognate pHLA complex. T cell-mediated killing of IGRP loaded K562 target cells was determined after 16 hours by flow cytometry with AV and PI staining. There was minimal K562 cell death in the absence of any T cells. $IGRP_{265\text{-}273}$ loaded K562 A2/PPI cells cultured with T-IGRP cells had significantly more AV^+/PI^+ cells than those cultured without T-IGRP cells. K562 PD-L1 cells were slightly resistant to T cell-mediated killing, with a 20% reduction in AV^+/PI^+ cells compared to K562 A2/PPI cells (Figure 7B). When K562 A2/PPI cells were co-cultured with T-IGRP cells and PD-L1 EVs, the percentage of AV^+/PI^+ cells was further reduced to approximately 40% of that in cultures without EVs (Figure 7B). This indicates that EV PD-L1 inhibited antigen-specific T cell-mediated killing of target cells, independent of any cell surface-presented PD-L1. Conversely, adding K-EVs to co-cultures with T-IGRP and K562 A2/PPI cells resulted in increased T cell-mediated killing of target cells (Figure 7C), consistent with our results in J-1E6 T cells showing increased T cell activation. In sum, these data suggest that EVs engineered to present pHLA and PD-L1 can promote immune tolerance against beta cells for T1D immunotherapy.

Discussion

EVs represent a potential therapeutic option for autoimmune diseases to impart many of the advantages of adoptively transferred cells while reducing some key limitations including cost, scalability, and patient risks from the transfer of living cells (*47-49*). While there is abundant

evidence that EVs influence immune outcomes (*9*), the mechanisms by which they influence T cell fate both *in vitro* and *in vivo* remain subject to debate (*15*). Some groups have shown that direct interactions occur between T cells and EVs *in vitro* (*35, 36*). Guo and colleagues performed a series of studies demonstrating that exosomes can directly suppress T cells through PD-1/PD-L1 interactions, but this was dependent on exosomal ICAM-1 (*50*). Conversely, other studies have shown that at least *in vitro*, APCs are required to stimulate T cells through EV uptake and cross-dressing of EV proteins onto the APC cell surface (*37, 38*), which is a process that has been previously studied (*51, 52*). It also remains possible that the K562 cells in our system are cross-presenting EV-delivered antigens through endogenous cell-expressed HLA-A2.

Our study investigated the effects of rationally engineered EVs in modulating T cell activation *in vitro*. We designed and validated a target:effector co-culture system with relevance to T1D, using engineered K562 cells as aAPCs and either modified Jurkat or primary human $CD8^+$ T cells as effectors. We showed that Jurkat T cells expressing CD8 and the 1E6 TCR clone respond specifically to PPI_{15-24} presented in HLA-A*02 in the presence of co-stimulation, as THP-1 cells loaded with PPI_{15-24} but lacking CD80 failed to induce IL-2 secretion from these cells. We also engineered PD-L1 into K562 cells and showed that this decreased T cell activation, even in the presence of excess exogenous peptide. Both K562 and THP-1 cells secreted EVs, which we were able to purify and use for functional studies in co-cultures with K562 and Jurkat T cells. In our system, K562 aAPCs internalized EVs during co-culture, and APCs were required for T cell activation by EVs. Additionally, we provide evidence that EV PD-L1 can inhibit T cell activation through aAPCs.

Of note, all EVs used for functional studies were isolated through a combination of ultrafiltration and BE-SEC, rather than the more traditional method of ultracentrifugation. This method allows for high reproducibility and scalability while also avoiding some pitfalls associated with ultracentrifugation, which is always limited by centrifuge rotor size and tube capacity and often results in unwanted biological contaminates (*30, 31, 53*). The specific BE-SEC configuration used for these studies was able to produce EVs on the order of 50 μg from a starting media volume of 200-300 ml. Due to lower levels of contaminating proteins, EV yields from chromatography separation tend to have higher purity in terms of μg protein/vesicle (*31*), providing an additional advantage over ultracentrifugation isolation.

An interesting observation that arose from our studies was the inability of EVs derived from THP-1 cells to impart the same stimulatory effects as K562-derived EVs in co-cultures with Jurkat T cells and K562 aAPCs, despite the presence of HLA on both EV populations, and excess exogenous PPI_{15-24} in the system. We suggest that a possible mechanism underlying this difference stems from the lack of CD80 on THP-1 cells and T-EVs. A very large dose of T-EVs did result in

a modest decrease in IL-2 secretion from J-1E6 cells. We speculate this was due to extensive HLA cross-dressing on K562 aAPCs, thus providing an overabundance of pHLA to T cells in the absence of proportional of CD80 co-stimulation. Thus, aAPCs treated with K-EVs are supplied with proportionate amounts of signals 1 (pHLA) and 2 (CD80) needed for T cell activation. While we hypothesize that differences in CD80 expression underlie the different effects observed from K-EV and T-EV, we also acknowledge that there are a myriad of other possible explanations as to why EVs from different cell sources are unable to elicit the same response from T cells. Lymphocytes (K562 cells) and monocytes (THP-1) perform distinct immune functions, and it thus follows that their EVs would perform distinct functions as well. Nonetheless, we posit that our data comparing the immune activity of EVs from different cell types could be a useful resource for the EV engineering community to guide EV engineering design criteria.

When designing and testing EVs containing PD-L1, we were initially focused on PD-1/PD-L1 interactions and the necessity of pHLA/TCR interactions for PD-1 signaling to occur (*54, 55*). However, the data we have with PD-L1 EVs from K562 and THP-1 cells suggests that CD80 also plays a role in EV-mediated T cell suppression through the APC cross-dressing pathway. The importance of EV CD80 has been demonstrated before, with increased CD80 leading to increased immune activation via dendritic cell cross-dressing (*56*) and decreased CD80 leading to a more regulatory immune state (*57*). Several groups have also shown that PD-L1 and CD80 interact on the same cell membrane to form *cis*-heterodimers, and this influences if and how these molecules can then bind to PD-1 and CD28 or CTLA-4 on other cell membranes (*43, 44*). Okazaki and colleagues have even demonstrated that disrupting *cis*-CD80/PD-L1 interactions alleviates multiple autoimmune disease models (*58*). As Jurkat T cells do not express CTLA-4 (*59, 60*), the interactions taking place in our model system would be between *cis*-CD80/PD-L1 and *trans*-PD-1/PD-L1. EV delivery of HLA to aAPCs remained consistent across all EV conditions with differences lying in co-delivery of PD-L1 and CD80, and only EVs co-delivering HLA, PD-L1, and CD80 able to significantly suppress T cell activation.

Delivery of nanoparticulate pMHC complexes has been previously demonstrated to impact T1D development. Santamaria and colleagues showed that synthetic nanoparticles coated with beta cell pMHC complexes are able to delay or prevent T1D progression in NOD mice (*61, 62*). While these studies demonstrated direct interactions between 40-60 nm nanoparticles and autoreactive T cells (*63*), others have shown that pMHC and anti-CD28 coated nanoparticles under 300 nm are unable to initiate TCR signaling events through such direct interactions due to their small size (*64*), similar to our observations with small EVs.

Overall, we showed that PD-L1-containing EVs were able to suppress T cell avatar-mediated, antigen-specific killing of target cells. One limitation of our approach is that the target cells used

in the cell-mediated lysis experiments were aAPCs loaded with peptide antigen. There is evidence that activated T cells can kill APCs (*65-67*), but future studies will be needed to determine whether our EVs are able to suppress killing of primary beta cells *in vivo*. Our system is HLA-specific and designed around human HLA-A2, thus typical mouse models of T1D are not suitable for *in vivo* testing of our EVs. There have been recent advances in transgenic mouse models such as the NOD-cMHC$^{-/-}$-A2 mouse strain, which is a humanized HLA model that spontaneously develops autoimmune diabetes (*68*). In this mouse model, classical mouse MHC class I variants H2-K^{d} and H2-D^{b} are deleted, and human HLA-A*02 is transgenically expressed. This model is therefore amenable to testing therapies such as ours that revolve around human HLA-A*02. One additional limitation is that our current product makes use of a known peptide antigen, which is not always possible in a polyclonal human autoimmune disease such as T1D. There is evidence in other systems of nanoparticulate-delivered pMHC complexes that a single antigen can produce a wider spread tolerance (*62*). Alternatively, many beta cell autoantigens naturally traffic to EVs (*21-23*) so primary beta cells could be used as EV producing factories if large enough numbers of human beta cells can be sourced, for example, via stem cell differentiation. Of relevance to our study, Eizirik and colleagues have shown that PD-L1 is expressed in insulin containing islets of people during early stages of T1D (*69*), and they as well as Fife and colleagues have demonstrated that inflammatory cytokines increase beta cell PD-L1 expression (*42, 69*). Thus, it may be possible that beta cells can be coerced to naturally release EVs containing autoantigens and PD-L1 during early stages of T1D, which could be an alternative strategy for generating tolerogenic EVs for use in a T1D setting.

The results presented here advance the understanding of the necessary conditions for EV-mediated T cell stimulation or inhibition, as well as considerations for engineering EVs for tissue-specific immune modulation. This approach for immune modulation combines the advantages of facile production of native HLA with the ability to engineer immune-regulatory functions in a plug-and-play fashion and is easily adaptable to other autoimmune diseases through delivery of different autoantigen pHLA complexes in EVs. In summary, EVs are a potentially unlimited source of nanoparticulate, multimeric, personalized HLA that can be both mass-produced and further engineered to fine-tune immunomodulatory capacity.

Materials and Methods

Cell culture. The chronic human mylogenous leukemia K562 cell line (*70*) (HLA null) was obtained from ATCC. K562 cells expressing HLA-A2, CD80, and CD83 were a gift from Drs. James Riley and Bruce Levine (University of Pennsylvania) and transduced with a lentivirus construct to express pre-proinsulin (PPI) in order to generate the K562 A2/PPI line. K562 A2/PPI

cells were further transduced with a lentivirus construct to express PD-L1 in order to generate K562 PD-L1 cells. Jurkat cells (ATCC, clone E6-1; TIB152™), a human T cell line (*71*), were transduced with lentiviral constructs containing CD8 and the PPI_{15-24}-reactive TCR (clone 1E6) (*34*). K562 and Jurkat cell lines were cultured in complete RPMI medium (cRPMI; RPMI-1640 containing L-glutamine supplemented with 10% fetal bovine serum [FBS], 1% penicillin-streptomycin, 10 mM HEPES, 1 mM sodium pyruvate, 1X non-essential amino acids, 0.2 μM 2-mercaptoethanol, final pH 7.4) and maintained at 37°C, 5% CO_2 atmosphere. THP-1 cells, a human acute monocytic leukemia cell line (*72*), were obtained from ATCC and maintained in RPMI containing L-glutamine supplemented with 10% FBS, 1% penicillin-streptomycin, 10 mM HEPES, 1 mM sodium pyruvate, 50 μM 2-mercaptoethanol, and 4.5 g/l glucose. THP-1 cells were supplemented with 100 U/ml recombinant human IFN-γ (BioLegend) for 3 days to induce PD-L1 expression. To generate EVs, K562 or THP-1 cells were cultured in T-150 flasks in their respective mediums, described above, made with EV-depleted FBS, which was prepared by centrifuging the FBS for 16 hours at 100,000 x g in a Beckman Coulter Optima L-90K Ultracentrifuge at 4°C. Medium was collected and replaced every 3 days, and cells were kept below 80% confluency. Conditioned medium from cells was stored at -80°C until EV isolation.

EV isolation via chromatography. Conditioned medium was thawed and centrifuged at 300 x g for 5 minutes to pellet cell debris. Supernatant was transferred to fresh tubes and centrifuged at 2,000 x g for 10 minutes to pellet larger extracellular particles. The supernatant was then passed through a 0.22 μm vacuum filter. Large volumes (up to 300 ml) of conditioned medium were concentrated through Sartorius Vivaspin 300 kDa molecular weight cut-off (MWCO) spin-filters at 2,500 x g for 3 minutes to a volume of less than 20 ml. Filtrate was discarded, and retentate was removed and saved in a separate tube. The concentrated conditioned medium was then loaded onto a HiScreen Capto Core 700 column connected to an ÄKTA Pure 25 L Chromatography system (Cytiva Life Sciences). Flow rate settings for column equilibration, sample loading, and column clean in place procedure were chosen according to the manufacturer's recommendations. The EV fraction was collected according to the 280 nm UV absorbance chromatogram and concentrated using Amicon Ultra-15 100 kDa MWCO spin-filters. Concentrated fractions were washed with 15 ml PBS in the same spin-filter and concentrated to a final volume of 150 μl. All spins and chromatography were performed at 4°C. Samples were stored at 4°C for no more than one week prior to use in functional assays.

EV isolation via ultracentrifugation. Conditioned medium was thawed and centrifuged at 300 x g for 5 minutes to pellet cell debris. Supernatant was transferred to fresh tubes and centrifuged at 2,000 x g for 10 minutes and at 16,500 x g for 20 minutes, followed by filtration through a 0.22 μm vacuum filter. EVs were pelleted by ultracentrifugation at 110,000 x g for 70

minutes in a Beckman Coulter Optima L-90K Ultracentrifuge. Pellets were resuspended in 1 mL PBS to wash and pelleted again at 120,000 x g for 75 minutes. After the wash, EVs pellets were resuspended in 150 μL PBS and stored until use. All spins were performed at 4°C. For short-term storage (< 1 week), samples were stored at 4°C. For longer-term storage, samples were stored at -80°C. All EVs isolated through ultracentrifugation were used for analysis of protein content and not functional studies.

Nanoparticle tracking analysis. Nanoparticle tracking analysis (NTA) was performed using a Nanosight LM14 (Malvern Instruments) consistent with methods previously described(*73*). EVs were diluted in PBS to a final concentration between 1:250 and 1:1000 prior to measurement to fit into the resolution window recommended by the manufacturer. Samples were loaded into the sample stage and the camera level was adjusted to 11 or 12. Three captures of 60 seconds each were recorded for each sample. Nanosight NTA 3.1 software was used to analyze particle size and concentration with a particle detection threshold at 2 or 3. Average particle concentrations measured by the software were multiplied by the dilution factor to obtain the final particle concentration for each sample.

Electron microscopy. EVs were examined by transmission electron microscopy negative stain at the UF Interdisciplinary Center for Biotechnology Research (ICBR) Electron Microscopy Core, RRID: SCR_019146. Poly-L-lysine treated, 400 mesh carbon coated Formvar copper grid was floated onto 3 μl of aliquoted EV suspension for 5 minutes, incubated on 2% paraformaldehyde in PBS (pH: 7.20) for 15 minutes, followed by a PBS wash and water wash for 5 minutes, each. Excess solution was drawn off with filter paper, and the grid was floated onto 1% aqueous uranyl acetate for 30 seconds. The stain was removed with filter paper, air dried and examined with a FEI Tecnai G2 Spirit Twin TEM (FEI Corp., Hillsboro, OR) operated at 120 kV. Digital images were acquired with a Gatan UltraScan 2k x 2k camera and Digital Micrograph software (Gatan Inc., Pleasanton, CA).

Western Blot Analysis. Total protein was extracted from cells using RIPA lysis buffer supplemented with Pierce Protease inhibitor tablets (Thermo Fisher Scientific). Protein content in cell lysates and EVs was determined using the Pierce BCA Protein Assay Kit (Thermo Fisher Scientific). Between 5 and 20 μg of total protein (kept consistent for individual experiments) was loaded into a 4-12% Bis-Tris gel, resolved by SDS-PAGE under reducing conditions, and transferred to a PVDF membrane. Membranes were blocked with Intercept PBS Blocking Buffer (Licor) for 1 hour, followed by incubation with primary antibodies overnight at 4°C. Membranes were washed 4 times for 5 minutes each with PBS + 0.1% Tween 20, incubated with IRDye© secondary antibodies (Licor) for 1 hour at room temperature and washed an additional 4 times. All blocking and antibody incubations were performed with gentle rocking. Membranes were imaged

using a Licor Odyssey Infrared Western Block Scanner. Antibody information is listed in Supplementary Table 1.

Lentiviral transduction of K562 and Jurkat cells. K562 cells expressing HLA-A2, CD80, and CD83 were transduced with lentiviral vectors to express human PPI and PD-L1. Pre-packaged PD-L1 lentivirus containing puromycin resistance was purchased from Vigene Biosciences (LH872950). PPI lentivirus was generated in-house from human PPI plasmid, which was a gift from Andrew Sewell (Cardiff University) and Mark Peakman (King's College London). Lentiviral vectors were used to express CD8 and the PPI-1E6 TCR (*74*) (both generated in-house) in human Jurkat T cells (J-1E6). Generation of all lentivirus constructs was performed as previously described (*75*). Transductions were carried out according to previously published protocols (*75*). Briefly, K562 or Jurkat T cells were seeded into a 24-well plate at 2.5 x 10^5 cells/well in 1 ml cRPMI and transduced in the presence of protamine sulfate (8 µg/ml, Sigma-Aldrich). Transgene expression was assessed 72 hours post-transduction by flow cytometry. To generate a stable PD-L1 expressing K562 cell line (K562 PD-L1), PD-$L1^+$ cells were sorted for on a BD FACS Aria III by PD-L1 surface staining (PD-L1 PE, clone 29E.2A3, BioLegend), then expanded *in vitro* in T-150 flasks in cRPMI for another week in the presence of 2 µg/ml puromycin before any functional studies or EV isolations.

Flow cytometry. Cells were stained with Live/Dead Near-IR Fixable Viability Dye (Thermo Fisher) according to the manufacturer's instructions. Next, cells were washed with FACS buffer (PBS + 2% FBS + 0.05% NaN_3) and incubated with Fc receptor blocking solution (Human TruStain FcX, BioLegend) for 5 minutes. Fluorophore conjugated antibodies (Supplementary Table 1) were directly added and incubated for 30 minutes in the dark at 4°C. Cells were washed twice and resuspended in FACS buffer and passed through a 35 µm strainer just before acquisition on a BD FACSCelesta flow cytometer. Marker positivity was set using single color-stained UltraComp eBeads (Thermo Fisher Scientific) and fluorescence minus one stained control cells. Analyses were performed using FlowJo software v10.6.2 (BD Life Sciences).

Extracellular vesicle PD-L1 analysis. PD-L1 was detected in K562 or THP-1 EVs using the Human PD-L1 DuoSet ELISA kit and DuoSet ELISA Ancillary Reagent Kit 2 (R&D Systems) according to the manufacturer's instructions. EVs were lysed prior to analysis using 1% Triton-X 100, and total protein content was measured using the Pierce BCA Protein Assay Kit.

Jurkat stimulation. K562 cells (either HLA null, A2/PPI, or PD-L1) were seeded in U-bottom 96 well plates at 1 x 10^5 cells/well in 100 µl cRPMI, then cultured for 4 hours in the presence of PPI_{15-24} (ALWGPDPAAA; kindly provided by Holger Russ, University of Colorado Denver) or $IGRP_{265-273}$ (VLFGLGFAI; Genscript) at 10 µg/ml to pre-load with exogenous peptide. Following this, J-1E6 T cells were added at 2 x 10^5 cells/well, along with any EV treatments (amounts

indicated in results and figures), in 100 µl for a final well volume of 200 µl. J-1E6 T cells cultured without K562 and peptide were used as a negative control, and those treated with 5 ng/ml phorbol 12-myristate 13-acetate (PMA) and 0.2 µM ionomycin were used a positive control. In some experiments, Jurkat 1E6 T cells were cultured with 10 µg/ml PPI_{15-24} peptide in the absence of K562 cells as an additional control. For experiments investigating CD80 blocking, CD80 blocking antibody (R&D Systems) or mouse IgG_1 isotype control antibody (Thermo Fisher Scientific) were added to co-cultures at a final concentration of 1 µg/ml. Co-cultures were performed in triplicate and incubated for 24 hours at 37°C, 5% CO_2 atmosphere, after which the culture supernatant was collected and stored at -80°C until analysis. The co-culture experiments were performed similarly with THP-1 cells replacing K562 cells, as indicated in the results section. Human IL-2 in the supernatant was measured using a sandwich ELISA kit (Human IL-2 Quantikine ELISA, R&D Systems) according to the manufacturer's instructions. The values for fold change in IL-2 secretion were calculated using the following formula:

$$FC_i = 1 + \frac{t_i - \bar{c}}{\bar{c}} \qquad (1)$$

where FC_i is the calculated fold change value, t_i is the measured IL-2 secretion of a technical replicate for a given EV treatment, and $\bar{c}$ is the average IL-2 secretion from the appropriate experimental positive control group.

Extracellular vesicle uptake assay. EVs from 300 ml of K562 A2/PPI conditioned medium were labeled with 1 µM DiR lipophilic dye (Thermo Fisher Scientific) for 15 minutes at room temperature after the first ultrafiltration step, but immediately prior to chromatography separation. Chromatography and subsequent ultrafiltration were then carried out as described above. K562 cells labeled with DiI (Thermo Fisher Scientific) were seeded into a 96 well-chambered coverslip (ibidi) at 1 x 10^5 cells/well in 100 µl cRPMI and pre-loaded for 4 hours with 10 µg/ml PPI_{15-24}. Following peptide loading, 4 x 10^{10} DiR-labeled EVs with or without 2 x 10^5 J-1E6 T cells (labeled with DiO) were added to wells containing peptide-loaded K562 cells in 150 µl for a final well volume of 250 µl. As a negative control, 2 x 10^5 J-1E6 cells and DiR-labeled EVs in 250 µl cRPMI were seeded in wells lacking K562 cells. Cultures were performed in duplicate and incubated for 24 hours at 37°C, 5% CO_2 atmosphere. Cells were imaged in the same 96 well-chambered coverslip using a Leica SP8 confocal microscope with HyD detectors, with a 20x/0.75 numerical aperture Plan-Apochromatic air objective.

Lentivirus production and transduction of primary human T cells. Peripheral blood mononuclear cells (PBMCs) were isolated from leukopheresis-enriched blood from healthy donors (median age: 27 years, range 20-27 years, N=3, 66% female) purchased from LifeSouth Community Blood Center (Gainesville, FL). Buffy coats were processed to isolate PBMCs via Ficoll density gradient centrifugation followed by naïve $CD8^+$ T cell isolation with EasySep Human Naïve $CD8^+$ T Cell Isolation Kit II (STEMCELL). Lentiviral vector encoding the Islet-specific Glucose-6-Phosphatase Catalytic Subunit 2 (IGRP)-reactive TCR (clone 32, $IGRP_{265-273}$-reactive) was produced as previously described (*76, 77*). Autoreactive $CD8^+$ T cell "avatars" expressing this TCR were generated as previously described (*75, 77*). Briefly, isolated naïve $CD8^+$ T cells were plated at 2.5 x 10^5 cells/well in a 24-well plate in 2 ml cRPMI on day 0 and activated with DynaBeads Human T-Activator anti-CD3/CD28 coated microbeads (Thermo Fisher Scientific) and recombinant human IL-2 (rIL-2; NCI Biological Resources Branch Preclinical Repository). After 48 hours incubation at 37C, 5% CO_2, cells were transduced with 3 transduction units (TU)/cell of lentivirus in the presence of 8 µg/ml protamine sulfate and 100IU rIL-2 and spinnoculated at 1,000 x g for 30 minutes at 32°C. Transduction efficiency was assessed by eGFP expression via flow cytometry 3-5 days post-transduction.

Cell mediated lysis assay. K562 A2/PPI cells were labeled with CellTrace Violet (CTV, Invitrogen) and seeded in a 48 well plate at 30,000 cells/well in 300 µl cRPMI. Twenty-four hours later, the cells were pre-loaded with 10 µg/ml $IGRP_{265-273}$ peptide for 4 hours. Then, IGRP T cell avatars were added to wells at a 5:1 target:effector ratio, with or without EVs from 300 mL of K562 PD-L1 conditioned medium for a final well volume of 600 µl. Co-cultures were incubated for 16 hours at 37°C, 5% CO_2, after which cells were collected into FACS tubes and stained with propidium iodide (PI, Invitrogen) and AlexaFluor 647-labeled Annexin-V (AV, BioLegend) in Annexin V binding buffer (BioLegend) according to the manufacturer's instructions. Cells were acquired on a BD FACSCelesta and analyzed using FlowJo software v10.6.2. The percent specific lysis of CTV^+ K562 cells was calculated as previously described (*78*).

Statistical analysis. All measurements were taken from distinct biological or technical replicates. Means among three or more groups were compared by one- or two-way analysis of variance (ANOVA) with Tukey's post-hoc pairwise comparison, and means between two groups were compared by two-tailed Student's *t* test in GraphPad Prism version 9 software. A linear mixed effects model in RStudio was used to determine statistical significance when comparing fold change in IL-2 across all experiments with EVs. This model was chosen over ANOVA due to the clustered data and unbalanced design across individual experiments. A confidence level of 95% was considered significant. The statistical test used, exact *P* values, and definition of *n* are indicated in the figure legends. Error bars display the mean ± standard error of the mean (SEM).

Acknowledgments

We would like to thank the UF ICBR Electron Microscopy Core, RRID:SCR019146, and Rudolfo Alvarado for performing electron microscopy.

Funding: This work was funded by
National Institutes of Health grant F31DK126397 (MWB)
National Institutes of Health grant T32DK108736 (MWB and LDP)
National Institutes of Health grant F31DK129004 (LDP)
National Institutes of Health grant R01DK132387 (EAP)
National Institutes of Health grant P01AI042288 (TMB EAP)
National Institutes of Health grant UH3DK122638 (TMB, EAP)

Author contributions: M.W.B., D.S., A.P., and E.A.P. performed experiments and data analysis. T.M. and L.D.P. provided reagents and discussions critical to the manuscript. T.M. and L.D.P. generated T cell avatars. T.M.B. provided critical expertise and support. M.W.B. and E.A.P. designed the study and wrote the manuscript. All authors discussed the results and commented on the manuscript. E.A.P. is the guarantor of this work and, as such, had full access to all data in the study and takes responsibility for the integrity of the data and the accuracy of the data analysis.

Competing interests: All other authors declare they have no competing interests.

Data and materials availability: All data needed to evaluate the conclusions in the paper are present in the paper and/or Supplementary Materials. All source data used to generate plots are available through the Figshare data repository under accession number 10.6084/m9.figshare.22250581.

References

1. G. van Niel, G. D'Angelo, G. Raposo, Shedding light on the cell biology of extracellular vesicles. *Nature Reviews Molecular Cell Biology* **19**, 213-228 (2018).
2. C. Théry, K. W. Witwer, E. Aikawa, M. J. Alcaraz, J. D. Anderson, R. Andriantsitohaina, . . . E. K. Zuba-Surma, Minimal information for studies of extracellular vesicles 2018 (MISEV2018): a position statement of the International Society for Extracellular Vesicles and update of the MISEV2014 guidelines. *Journal of Extracellular Vesicles* **7**, 1535750 (2018).
3. K. W. Witwer, C. Théry, Extracellular vesicles or exosomes? On primacy, precision, and popularity influencing a choice of nomenclature. *Journal of Extracellular Vesicles* **8**, 1648167 (2019).
4. R. Kalluri, V. S. LeBleu, The biology, function, and biomedical applications of exosomes. *Science* **367**, eaau6977 (2020).

5. M. Harmati, M. Bukva, T. Böröczky, K. Buzás, E. Gyukity-Sebestyén, The role of the metabolite cargo of extracellular vesicles in tumor progression. *Cancer and Metastasis Reviews* **40**, 1203-1221 (2021).
6. M. Mathieu, L. Martin-Jaular, G. Lavieu, C. Théry, Specificities of secretion and uptake of exosomes and other extracellular vesicles for cell-to-cell communication. *Nature Cell Biology* **21**, 9-17 (2019).
7. J. Meldolesi, Exosomes and Ectosomes in Intercellular Communication. *Curr Biol* **28**, R435-r444 (2018).
8. T. Skotland, K. Sandvig, A. Llorente, Lipids in exosomes: Current knowledge and the way forward. *Progress in Lipid Research* **66**, 30-41 (2017).
9. C. Thery, M. Ostrowski, E. Segura, Membrane vesicles as conveyors of immune responses. *Nat Rev Immunol* **9**, 581-593 (2009).
10. T. Smyth, K. Petrova, N. M. Payton, I. Persaud, J. S. Redzic, M. W. Graner, . . . T. J. Anchordoquy, Surface functionalization of exosomes using click chemistry. *Bioconjug Chem* **25**, 1777-1784 (2014).
11. N. Yim, S.-W. Ryu, K. Choi, K. R. Lee, S. Lee, H. Choi, . . . C. Choi, Exosome engineering for efficient intracellular delivery of soluble proteins using optically reversible protein–protein interaction module. *Nature Communications* **7**, 12277 (2016).
12. Z. Zhao, J. McGill, P. Gamero-Kubota, M. He, Microfluidic on-demand engineering of exosomes towards cancer immunotherapy. *Lab on a Chip* **19**, 1877-1886 (2019).
13. J. P. K. Armstrong, M. N. Holme, M. M. Stevens, Re-Engineering Extracellular Vesicles as Smart Nanoscale Therapeutics. *ACS Nano* **11**, 69-83 (2017).
14. I. V. Miller, T. G. P. Grunewald, Tumour-derived exosomes: Tiny envelopes for big stories. *Biology of the Cell* **107**, 287-305 (2015).
15. D. Turpin, M.-E. Truchetet, B. Faustin, J.-F. Augusto, C. Contin-Bordes, A. Brisson, . . . P. Duffau, Role of extracellular vesicles in autoimmune diseases. *Autoimmunity Reviews* **15**, 174-183 (2016).
16. G. Chen, A. C. Huang, W. Zhang, G. Zhang, M. Wu, W. Xu, . . . W. Guo, Exosomal PD-L1 contributes to immunosuppression and is associated with anti-PD-1 response. *Nature* **560**, 382-386 (2018).
17. D. Daassi, K. M. Mahoney, G. J. Freeman, The importance of exosomal PDL1 in tumour immune evasion. *Nat Rev Immunol* **20**, 209-215 (2020).
18. E. Hui, J. Cheung, J. Zhu, X. Su, M. J. Taylor, H. A. Wallweber, . . . R. D. Vale, T cell costimulatory receptor CD28 is a primary target for PD-1–mediated inhibition. *Science* **355**, 1428-1433 (2017).
19. H. Arasanz, M. Gato-Cañas, M. Zuazo, M. Ibañez-Vea, K. Breckpot, G. Kochan, D. Escors, PD1 signal transduction pathways in T cells. *Oncotarget* **8**, 51936-51945 (2017).
20. M. Poggio, T. Hu, C.-C. Pai, B. Chu, C. D. Belair, A. Chang, . . . R. Blelloch, Suppression of Exosomal PD-L1 Induces Systemic Anti-tumor Immunity and Memory. *Cell* **177**, 414-427.e413 (2019).
21. C. P. Hasilo, S. Negi, I. Allaeys, N. Cloutier, A. K. Rutman, M. Gasparrini, . . . S. Paraskevas, Presence of diabetes autoantigens in extracellular vesicles derived from human islets. *Scientific Reports* **7**, 5000 (2017).
22. A. N. Vomund, B. H. Zinselmeyer, J. Hughes, B. Calderon, C. Valderrama, S. T. Ferris, . . . E. R. Unanue, Beta cells transfer vesicles containing insulin to phagocytes for presentation to T cells. *Proc Natl Acad Sci U S A* **112**, E5496-5502 (2015).

23. C. Cianciaruso, E. A. Phelps, M. Pasquier, R. Hamelin, D. Demurtas, M. Alibashe Ahmed, . . . S. Baekkeskov, Primary Human and Rat beta-Cells Release the Intracellular Autoantigens GAD65, IA-2, and Proinsulin in Exosomes Together With Cytokine-Induced Enhancers of Immunity. *Diabetes* **66**, 460-473 (2017).
24. J. A. Noble, Immunogenetics of type 1 diabetes: A comprehensive review. *J Autoimmun* **64**, 101-112 (2015).
25. A. W. Purcell, S. Sechi, T. P. DiLorenzo, The Evolving Landscape of Autoantigen Discovery and Characterization in Type 1 Diabetes. *Diabetes* **68**, 879-886 (2019).
26. A. M. Anderson, L. G. Landry, A. A. Alkanani, L. Pyle, A. C. Powers, M. A. Atkinson, . . . M. Nakayama, Human islet T cells are highly reactive to preproinsulin in type 1 diabetes. *Proceedings of the National Academy of Sciences* **118**, e2107208118 (2021).
27. M. O. Butler, N. Hirano, Human cell-based artificial antigen-presenting cells for cancer immunotherapy. *Immunological Reviews* **257**, 191-209 (2014).
28. C. Théry, S. Amigorena, G. Raposo, A. Clayton, Isolation and Characterization of Exosomes from Cell Culture Supernatants and Biological Fluids. *Current Protocols in Cell Biology* **30**, 3.22.21-23.22.29 (2006).
29. R. Linares, S. Tan, C. Gounou, N. Arraud, A. R. Brisson, High-speed centrifugation induces aggregation of extracellular vesicles. *Journal of Extracellular Vesicles* **4**, 29509 (2015).
30. J. Z. Nordin, Y. Lee, P. Vader, I. Mäger, H. J. Johansson, W. Heusermann, . . . S. E. L. Andaloussi, Ultrafiltration with size-exclusion liquid chromatography for high yield isolation of extracellular vesicles preserving intact biophysical and functional properties. *Nanomedicine: Nanotechnology, Biology and Medicine* **11**, 879-883 (2015).
31. G. Corso, I. Mäger, Y. Lee, A. Görgens, J. Bultema, B. Giebel, . . . S. E. L. Andaloussi, Reproducible and scalable purification of extracellular vesicles using combined bind-elute and size exclusion chromatography. *Scientific Reports* **7**, 11561 (2017).
32. F. G. Kugeratski, K. Hodge, S. Lilla, K. M. McAndrews, X. Zhou, R. F. Hwang, . . . R. Kalluri, Quantitative proteomics identifies the core proteome of exosomes with syntenin-1 as the highest abundant protein and a putative universal biomarker. *Nature Cell Biology* **23**, 631-641 (2021).
33. Y. Wu, W. Deng, D. J. Klinke Ii, Exosomes: improved methods to characterize their morphology, RNA content, and surface protein biomarkers. *Analyst* **140**, 6631-6642 (2015).
34. A. Skowera, R. J. Ellis, R. Varela-Calviño, S. Arif, G. C. Huang, C. Van-Krinks, . . . M. Peakman, CTLs are targeted to kill β cells in patients with type 1 diabetes through recognition of a glucose-regulated preproinsulin epitope. *The Journal of Clinical Investigation* **118**, 3390-3402 (2008).
35. C. Admyre, S. M. Johansson, S. Paulie, S. Gabrielsson, Direct exosome stimulation of peripheral human T cells detected by ELISPOT. *Eur J Immunol* **36**, 1772-1781 (2006).
36. E. N. M. Nolte-‘t Hoen, S. I. Buschow, S. M. Anderton, W. Stoorvogel, M. H. M. Wauben, Activated T cells recruit exosomes secreted by dendritic cells via LFA-1. *Blood* **113**, 1977-1981 (2009).
37. J. Marino, M. H. Babiker-Mohamed, P. Crosby-Bertorini, J. T. Paster, C. LeGuern, S. Germana, . . . G. Benichou, Donor exosomes rather than passenger leukocytes initiate alloreactive T cell responses after transplantation. *Sci Immunol* **1**, (2016).

38. A. Prunevieille, M. H. Babiker-Mohamed, C. Aslami, B. Gonzalez-Nolasco, N. Mooney, G. Benichou, T cell antigenicity and immunogenicity of allogeneic exosomes. *American Journal of Transplantation* **21**, 2583-2589 (2021).
39. J. Monypenny, H. Milewicz, F. Flores-Borja, G. Weitsman, A. Cheung, R. Chowdhury, . . . T. Ng, ALIX Regulates Tumor-Mediated Immunosuppression by Controlling EGFR Activity and PD-L1 Presentation. *Cell Reports* **24**, 630-641 (2018).
40. S. Chen, G. A. Crabill, T. S. Pritchard, T. L. McMiller, P. Wei, D. M. Pardoll, . . . S. L. Topalian, Mechanisms regulating PD-L1 expression on tumor and immune cells. *Journal for ImmunoTherapy of Cancer* **7**, 305 (2019).
41. K. Sri-ngern-ngam, P. Keawvilai, T. Pisitkun, T. Palaga, Upregulation of programmed cell death 1 by interferon gamma and its biological functions in human monocytes. *Biochemistry and Biophysics Reports* **32**, 101369 (2022).
42. K. C. Osum, A. L. Burrack, T. Martinov, N. L. Sahli, J. S. Mitchell, C. G. Tucker, . . . B. T. Fife, Interferon-gamma drives programmed death-ligand 1 expression on islet beta cells to limit T cell function during autoimmune diabetes. *Sci Rep* **8**, 8295 (2018).
43. D. Sugiura, T. Maruhashi, I.-m. Okazaki, K. Shimizu, T. K. Maeda, T. Takemoto, T. Okazaki, Restriction of PD-1 function by cis-PD-L1/CD80 interactions is required for optimal T cell responses. *Science* **364**, 558-566 (2019).
44. Y. Zhao, C. K. Lee, C.-H. Lin, R. B. Gassen, X. Xu, Z. Huang, . . . E. Hui, PD-L1:CD80 Cis-Heterodimer Triggers the Co-stimulatory Receptor CD28 While Repressing the Inhibitory PD-1 and CTLA-4 Pathways. *Immunity* **51**, 1059-1073.e1059 (2019).
45. D. M. Sansom, L. S. K. Walker, Dimers Aren't Forever: CD80 Breaks up with PD-L1. *Immunity* **51**, 972-974 (2019).
46. I. Jarchum, L. Nichol, M. Trucco, P. Santamaria, T. P. DiLorenzo, Identification of novel IGRP epitopes targeted in type 1 diabetes patients. *Clinical Immunology* **127**, 359-365 (2008).
47. R. C. Sterner, R. M. Sterner, CAR-T cell therapy: current limitations and potential strategies. *Blood Cancer Journal* **11**, 69 (2021).
48. V. Janelle, J.-S. Delisle, T-Cell Dysfunction as a Limitation of Adoptive Immunotherapy: Current Concepts and Mitigation Strategies. *Cancers* **13**, 598 (2021).
49. R. Borgert, Improving outcomes and mitigating costs associated with CAR T-cell therapy. *Am J Manag Care* **27**, S253-s261 (2021).
50. W. Zhang, W. Zhong, B. Wang, J. Yang, J. Yang, Z. Yu, . . . W. Guo, ICAM-1-mediated adhesion is a prerequisite for exosome-induced T cell suppression. *Developmental Cell* **57**, 329-343.e327 (2022).
51. K. O'Brien, S. Ughetto, S. Mahjoum, A. V. Nair, X. O. Breakefield, Uptake, functionality, and re-release of extracellular vesicle-encapsulated cargo. *Cell Reports* **39**, 110651 (2022).
52. T. Tian, Y. Wang, H. Wang, Z. Zhu, Z. Xiao, Visualizing of the cellular uptake and intracellular trafficking of exosomes by live-cell microscopy. *J Cell Biochem* **111**, 488-496 (2010).
53. Y. Yang, Y. Wang, S. Wei, C. Zhou, J. Yu, G. Wang, . . . L. Zhao, Extracellular vesicles isolated by size-exclusion chromatography present suitability for RNomics analysis in plasma. *Journal of Translational Medicine* **19**, 104 (2021).
54. T. Pentcheva-Hoang, L. Chen, D. M. Pardoll, J. P. Allison, Programmed death-1 concentration at the immunological synapse is determined by ligand affinity and availability. *Proceedings of the National Academy of Sciences* **104**, 17765-17770 (2007).

55. T. Yokosuka, M. Takamatsu, W. Kobayashi-Imanishi, A. Hashimoto-Tane, M. Azuma, T. Saito, Programmed cell death 1 forms negative costimulatory microclusters that directly inhibit T cell receptor signaling by recruiting phosphatase SHP2. *The Journal of Experimental Medicine* **209**, 1201-1217 (2012).
56. W. Hu, F. Huang, L. Ning, J. Hao, J. Wan, S. Hao, Enhanced immunogenicity of leukemia-derived exosomes via transfection with lentiviral vectors encoding costimulatory molecules. *Cellular Oncology* **43**, 889-900 (2020).
57. W. Yin, S. Ouyang, Z. Luo, Q. Zeng, B. Hu, L. Xu, . . . H. Yang, Immature Exosomes Derived from MicroRNA-146a Overexpressing Dendritic Cells Act as Antigen-Specific Therapy for Myasthenia Gravis. *Inflammation* **40**, 1460-1473 (2017).
58. D. Sugiura, I.-m. Okazaki, T. K. Maeda, T. Maruhashi, K. Shimizu, R. Arakaki, . . . T. Okazaki, PD-1 agonism by anti-CD80 inhibits T cell activation and alleviates autoimmunity. *Nature Immunology* **23**, 399-410 (2022).
59. T. Lindsten, K. P. Lee, E. S. Harris, B. Petryniak, N. Craighead, P. J. Reynolds, . . . C. H. June, Characterization of CTLA-4 structure and expression on human T cells. *J Immunol* **151**, 3489-3499 (1993).
60. G. J. Freeman, D. B. Lombard, C. D. Gimmi, S. A. Brod, K. Lee, J. C. Laning, . . . L. M. Nadler, CTLA-4 and CD28 mRNA are coexpressed in most T cells after activation. Expression of CTLA-4 and CD28 mRNA does not correlate with the pattern of lymphokine production. *J Immunol* **149**, 3795-3801 (1992).
61. S. Tsai, A. Shameli, J. Yamanouchi, X. Clemente-Casares, J. Wang, P. Serra, . . . P. Santamaria, Reversal of Autoimmunity by Boosting Memory-like Autoregulatory T Cells. *Immunity* **32**, 568-580 (2010).
62. X. Clemente-Casares, J. Blanco, P. Ambalavanan, J. Yamanouchi, S. Singha, C. Fandos, . . . P. Santamaria, Expanding antigen-specific regulatory networks to treat autoimmunity. *Nature* **530**, 434 (2016).
63. S. Singha, K. Shao, Y. Yang, X. Clemente-Casares, P. Sole, A. Clemente, . . . P. Santamaria, Peptide-MHC-based nanomedicines for autoimmunity function as T-cell receptor microclustering devices. *Nat Nanotechnol* **12**, 701-710 (2017).
64. J. W. Hickey, F. P. Vicente, G. P. Howard, H. Q. Mao, J. P. Schneck, Biologically Inspired Design of Nanoparticle Artificial Antigen-Presenting Cells for Immunomodulation. *Nano Lett* **17**, 7045-7054 (2017).
65. G. T. Belz, L. Zhang, M. D. H. Lay, F. Kupresanin, M. P. Davenport, Killer T cells regulate antigen presentation for early expansion of memory, but not naive, CD8+ T cell. *Proceedings of the National Academy of Sciences* **104**, 6341-6346 (2007).
66. I. F. Hermans, D. S. Ritchie, J. Yang, J. M. Roberts, F. Ronchese, CD8+ T Cell-Dependent Elimination of Dendritic Cells In Vivo Limits the Induction of Antitumor Immunity1. *The Journal of Immunology* **164**, 3095-3101 (2000).
67. S. N. Mueller, C. M. Jones, A. T. Stock, M. Suter, W. R. Heath, F. R. Carbone, CD4+ T Cells Can Protect APC from CTL-Mediated Elimination1. *The Journal of Immunology* **176**, 7379-7384 (2006).
68. T. Takaki, M. P. Marron, C. E. Mathews, S. T. Guttmann, R. Bottino, M. Trucco, . . . D. V. Serreze, HLA-A*0201-Restricted T Cells from Humanized NOD Mice Recognize Autoantigens of Potential Clinical Relevance to Type 1 Diabetes. *The Journal of Immunology* **176**, 3257-3265 (2006).

69. M. L. Colli, J. L. E. Hill, L. Marroquí, J. Chaffey, R. S. Dos Santos, P. Leete, . . . D. L. Eizirik, PDL1 is expressed in the islets of people with type 1 diabetes and is up-regulated by interferons alpha and gamma via IRF1 induction. *EBioMedicine* **36**, 367-375 (2018).
70. C. B. Lozzio, B. B. Lozzio, Human Chronic Myelogenous Leukemia Cell-Line With Positive Philadelphia Chromosome. *Blood* **45**, 321-334 (1975).
71. U. Schneider, H.-U. Schwenk, G. Bornkamm, Characterization of EBV-genome negative "null" and "T" cell lines derived from children with acute lymphoblastic leukemia and leukemic transformed non-Hodgkin lymphoma. *International Journal of Cancer* **19**, 621-626 (1977).
72. S. Tsuchiya, M. Yamabe, Y. Yamaguchi, Y. Kobayashi, T. Konno, K. Tada, Establishment and characterization of a human acute monocytic leukemia cell line (THP-1). *International Journal of Cancer* **26**, 171-176 (1980).
73. R. A. Dragovic, C. Gardiner, A. S. Brooks, D. S. Tannetta, D. J. P. Ferguson, P. Hole, . . . I. L. Sargent, Sizing and phenotyping of cellular vesicles using Nanoparticle Tracking Analysis. *Nanomedicine: Nanotechnology, Biology and Medicine* **7**, 780-788 (2011).
74. A. M. Bulek, D. K. Cole, A. Skowera, G. Dolton, S. Gras, F. Madura, . . . A. K. Sewell, Structural basis for the killing of human beta cells by CD8+ T cells in type 1 diabetes. *Nature Immunology* **13**, 283-289 (2012).
75. W. I. Yeh, H. R. Seay, B. Newby, A. L. Posgai, F. B. Moniz, A. Michels, . . . T. M. Brusko, Avidity and Bystander Suppressive Capacity of Human Regulatory T Cells Expressing De Novo Autoreactive T-Cell Receptors in Type 1 Diabetes. *Front Immunol* **8**, 1313 (2017).
76. A. Ventura, A. Meissner, C. P. Dillon, M. McManus, P. A. Sharp, L. Van Parijs, . . . T. Jacks, Cre-lox-regulated conditional RNA interference from transgenes. *Proceedings of the National Academy of Sciences* **101**, 10380-10385 (2004).
77. B. N. Newby, T. M. Brusko, B. Zou, M. A. Atkinson, M. Clare-Salzler, C. E. Mathews, Type 1 Interferons Potentiate Human CD8(+) T-Cell Cytotoxicity Through a STAT4- and Granzyme B-Dependent Pathway. *Diabetes* **66**, 3061-3071 (2017).
78. J. W. Dean, L. D. Peters, C. A. Fuhrman, H. R. Seay, A. L. Posgai, S. E. Stimpson, . . . T. M. Brusko, Innate inflammation drives NK cell activation to impair Treg activity. *Journal of Autoimmunity* **108**, 102417 (2020).

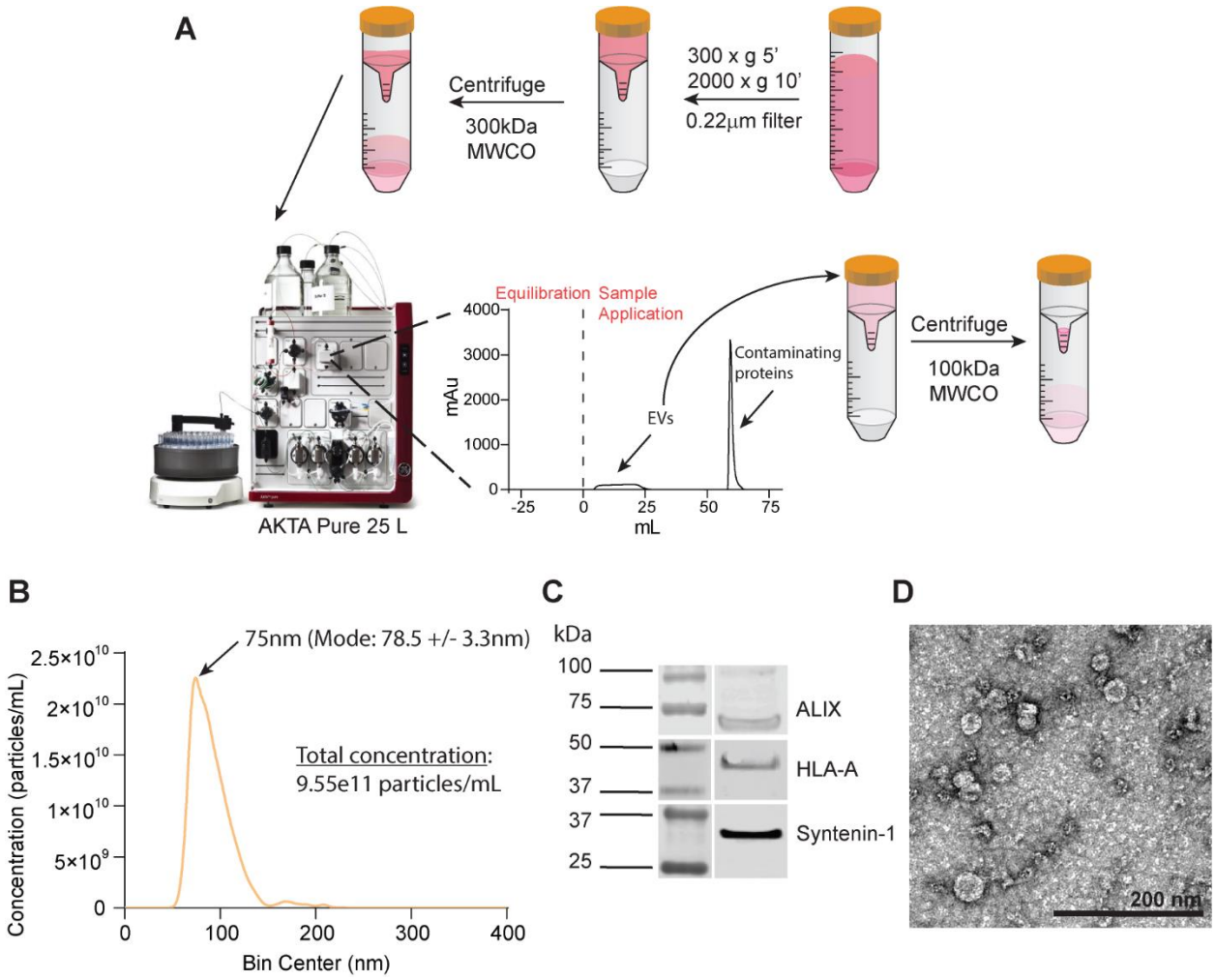

Figure 1. EV isolation and characterization. (A) Schematic overview of the workflow. Conditioned media is processed through low-speed centrifugation and vacuum filtration to remove cells and cellular debris, then filtered through 300kDa MWCO UF devices to remove soluble proteins and concentrate the EV fraction. Concentrated media is loaded onto a BE-SEC column using the ÄKTA Pure chromatography system. The first eluting fractions (EVs) are collected via an automated fraction collector then subsequently concentrated using 100kDa MWCO UF devices and used for further experiments. Contaminating proteins trapped by the BE-SEC column are eluted out during the column wash. (B) NTA showing representative particle concentration and size distribution of EVs derived from K562 A2/PPI cells. (C) Western blot analysis of EV isolates from K562 A2/PPI cells demonstrating the presence of small EV markers. n=3 (D) Representative TEM image of K562 A2/PPI cell-derived EVs. Scale bar = 200nm.

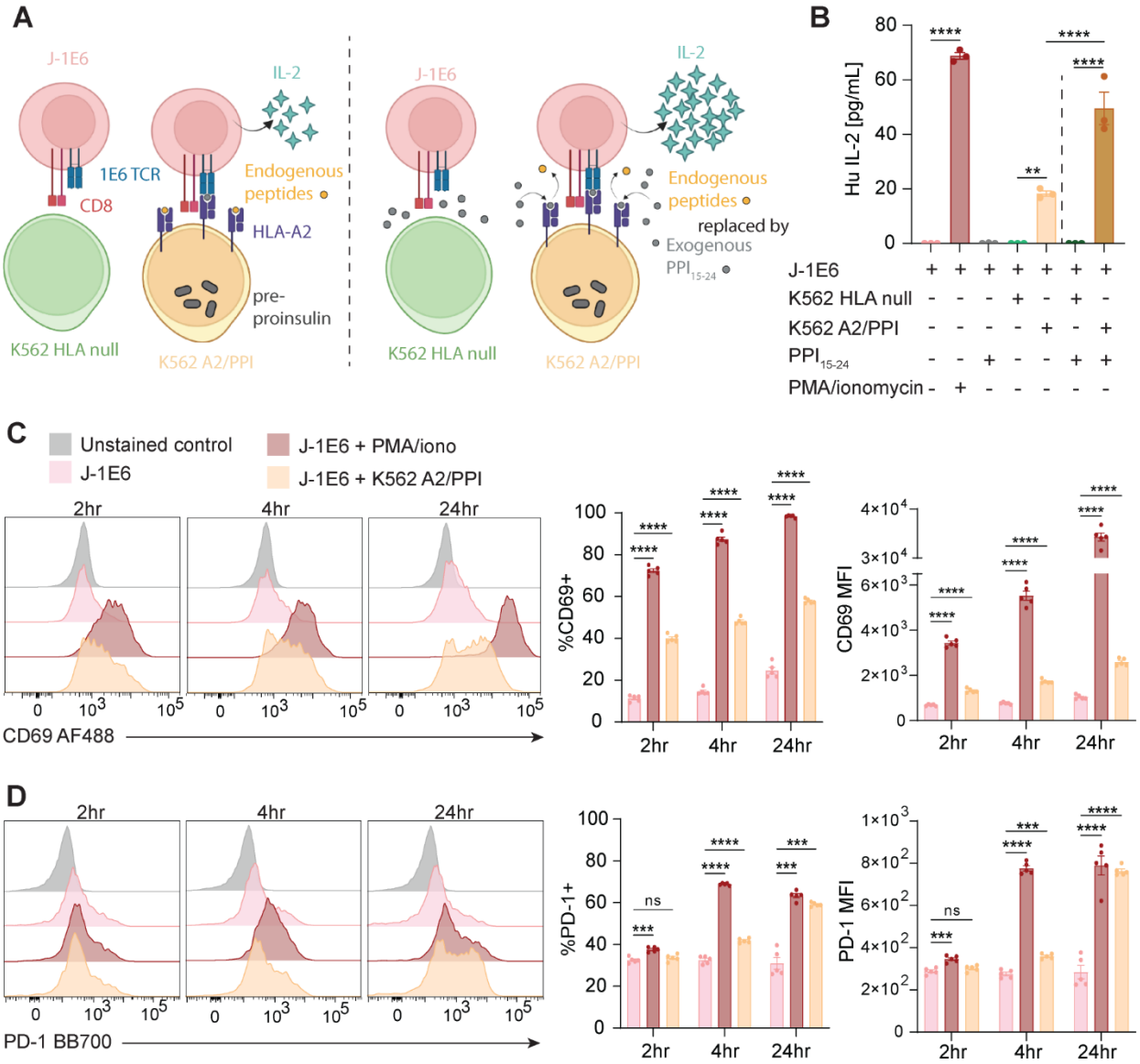

Figure 2. Validating an *in vitro* target:effector co-culture model for EV engineering. (A) Schematic representation of J-1E6 and K562 co-culture. Yellow and gray circles represent endogenous peptides presented in HLA-A2 and exogenous PPI_{15-24} added into the co-culture system, respectively. (B) IL-2 secretion from J-1E6 T cells showing activation from K562 A2/PPI cells, which is increased with exogenous peptide loading in HLA-A*02. K562 cells lacking HLA-A*02 fail to induce IL-2 secretion from J-1E6 T cells even in the presence of exogenous peptide. n = 3. Representative of 4 independent experiments. (C) Surface expression of the activation marker CD69 on J-1E6 T cells over a 24 hour co-culture with K562 A2/PPI cells. n = 5. (D) Surface expression of PD-1 on J-1E6 T cells over a 24 hour co-culture with K562 A2/PPI cells. n = 5. Statistical differences for (B) were determined by one-way ANOVA followed by Tukey's multiple comparisons test. Statistical differences for (C) and (D) were determined by two-way ANOVA followed by Tukey's multiple comparisons test. ns = non-significant, ** $p < 0.01$, *** $p < 0.001$, **** $p < 0.0001$. Panel (A) was created using Biorender.com.

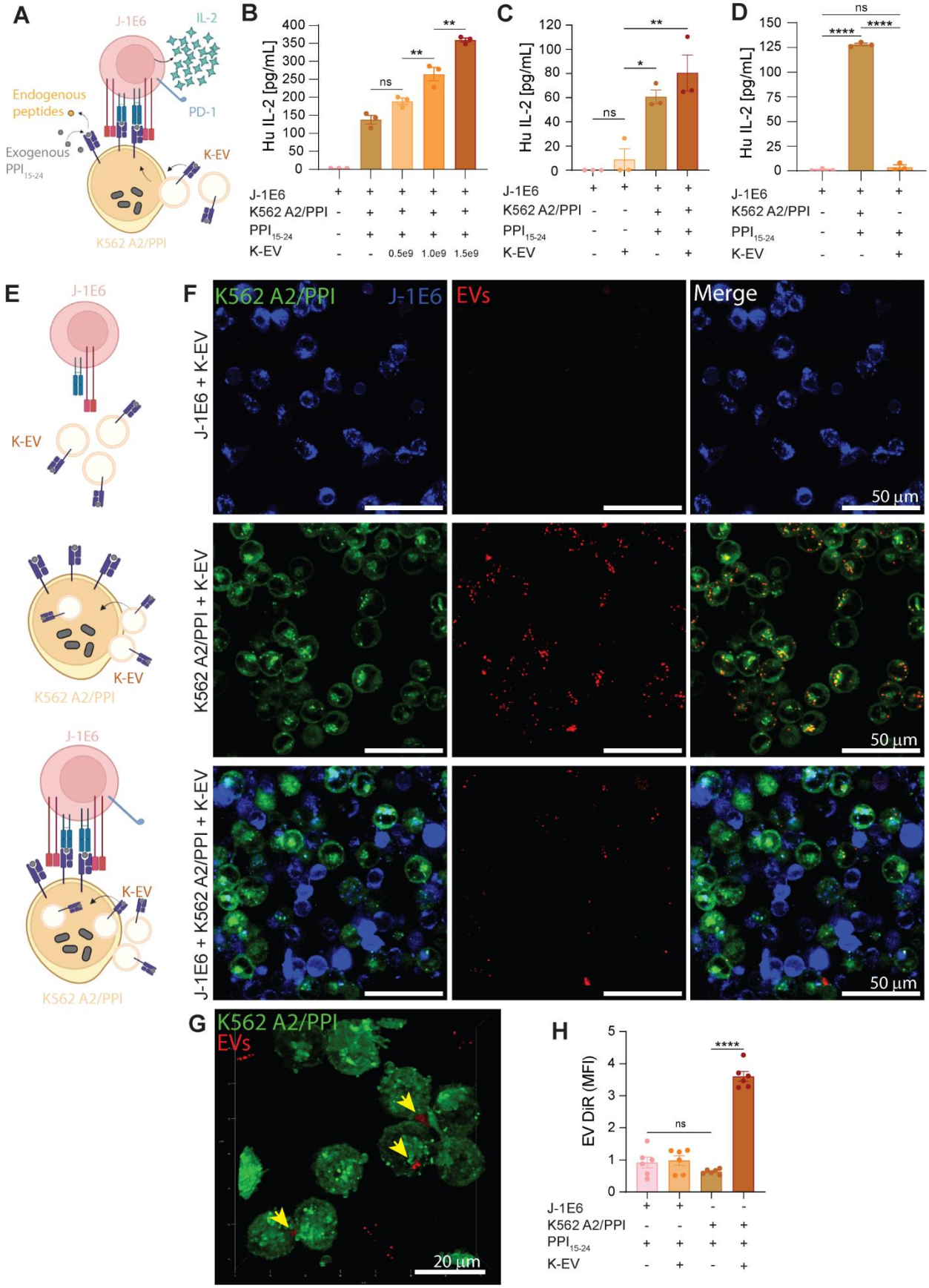
A
J-1E6
IL-2
Endogenous peptides
PD-1
Exogenous PPI15-24
K-EV
K562 A2/PPI
B
Hu IL-2 [pg/mL]
ns
**
**
J-1E6
K562 A2/PPI
PPI15-24
K-EV
0.5e9
1.0e9
1.5e9
C
Hu IL-2 [pg/mL]
ns
*
**
D
Hu IL-2 [pg/mL]
ns
****
****
E
J-1E6
K-EV
K562 A2/PPI
F
K562 A2/PPI
J-1E6
EVs
Merge
J-1E6 + K-EV
K562 A2/PPI + K-EV
J-1E6 + K562 A2/PPI + K-EV
50 µm
G
K562 A2/PPI
EVs
20 µm
H
EV DiR (MFI)
ns
****

Figure 3 EVs need APCs to modulate T cell activation *in vitro*. (A) Schematic representation of J-1E6 co-culture with K562 A2/PPI cells and K-EVs. (B) IL-2 secretion from J-1E6 T cells showing increased activation with increasing amounts of K-EVs in cultures. Representative of 5 independent experiments. (C) IL-2 secretion from J-1E6 T cells after co-culture with K562 A2/PPI cells and/or EVs, showing that EVs alone do not activate T cells. n = 3. (D) IL-2 secretion from J-1E6 cells after co-culture with K562 A2/PPI cells or EVs, showing that EVs in the presence of exogenous PPI_{15-24} do not activate T cells. Representative of 4 independent experiments. (E) Schematic representations of the different conditions used in (F) to determine EV interactions in the co-culture system. (F) Confocal microscopy images of DiR-labeled K-EVs incubated with either DiI-labeled J-1E6, DiO-labeled K562 A2/PPI, or both cell types for 24 hours. DiR signal was detected in cultures with K562 A2/PPI cells and J-1E6 with K562 A2/PPI cells, but not J-1E6 cells alone, suggesting that K562 A2/PPI cells endocytose EVs. Representative of 2 independent experiments. (G) A high-resolution, 3D micrograph of K562 A2/PPI cells incubated with DiR-labeled K-EV. Yellow arrows indicate cell surface-bound EV clusters. (H) Mean fluorescent intensity (MFI) quantification of confocal microscopy images, showing higher DiR EV signal in K562 A2/PPI cells and no significant difference between J-1E6 cells with or without K-EV co-incubation. Each data point represents quantification from one image, with three images taken from each of two wells. Statistical differences for (B) through (D) and (H) were determined by one-way ANOVA followed by Tukey's multiple comparisons test. ns = non-significant, ** $p < 0.01$, **** $p < 0.0001$. Panels (A) and (E) were created using Biorender.com.

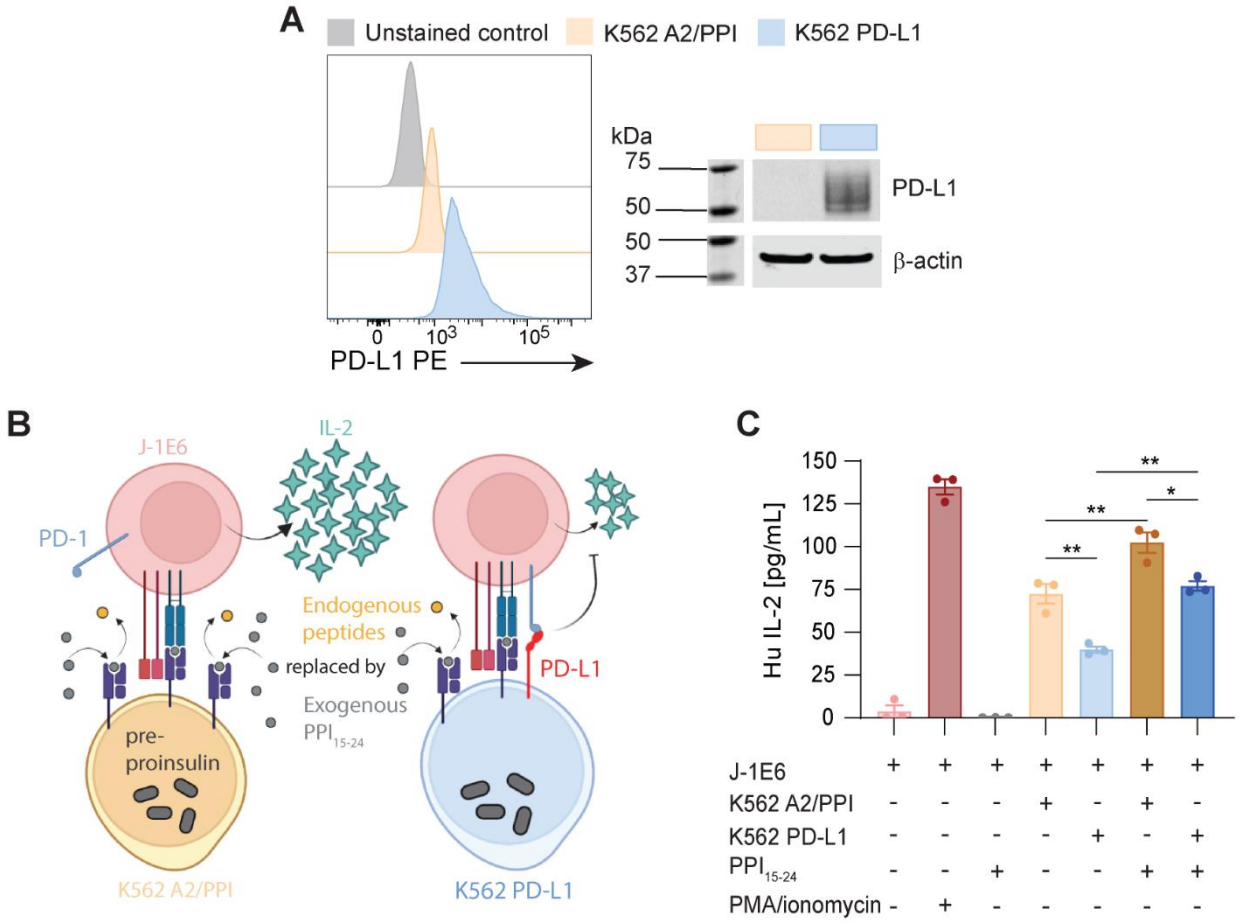

Figure 4. Driving PD-L1 expression in EV parent cells. (A) Surface expression of PD-L1 on lentivirus-transduced cells shown via flow cytometry, and further confirmed by western blot analysis. (B) Schematic representation of J-1E6 co-culture with either K562 A2/PPI or K562 PD-L1 cells, where PD-L1 engages with PD-1 to suppress IL-2 secretion. (C) IL-2 secretion from J-1E6 T cells showing decreased activation when co-cultured with K562 PD-L1 cells compared to K562 A2/PPI. This suppression is still seen when exogenous PPI_{15-24} is added to co-cultures. Representative of 9 independent experiments. Statistical differences for (C) were determined by one-way ANOVA followed by Tukey's multiple comparison test. * $p < 0.05$, ** $p < 0.01$. Panel (B) was created using Biorender.com.

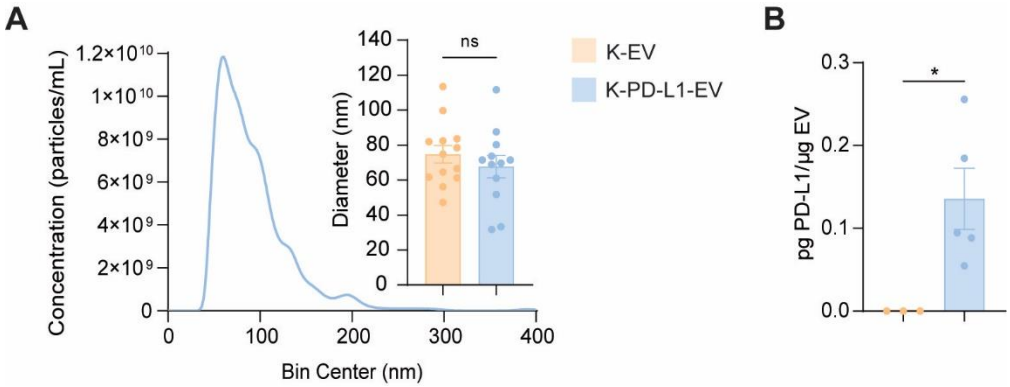

Figure 5. Validating PD-L1 expression in EVs. (A) NTA showing representative particle concentration and size distribution of EVs derived from K562 PD-L1 cells. The inset shows the mode particle diameter for multiple K-EV and K-PD-L1-EV preparations, indicating that lentiviral transduction did not negatively impact EV generation. n = 13 and n = 12. (B) ELISA of PD-L1 on EVs from K562 cells compared to total EV protein content. n = 5. Data from 2 independent experiments. Statistical differences for (A) and (B) were determined by an unpaired, two-tailed t-test. ns = non-significant, * $p < 0.05$.

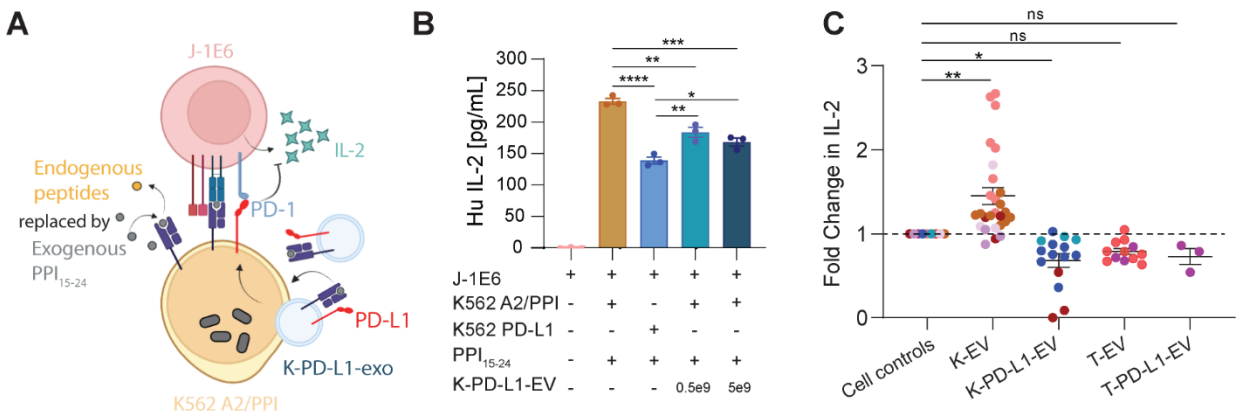

Fig. 6. K-PD-L1-EVs suppress T cell activation. (A) Schematic representation of J-1E6 co-cultures with K562 A2/PPI cells and K-PD-L1-EVs. (B) IL-2 secretion from J-1E6 cells showing decreased activation with K562 PD-L1 cells or increasing amounts of K-PD-L1-EVs in cultures, n = 3. Data shown are representative of 3 independent experiments. (C) Fold change in IL-2 secretion across all experiments with different exosome treatments, showing that K-EVs significantly increase and K-PD-L1-EVs significantly decrease IL-2 secretion. T-EVs and T-PD-L1-EVs have no significant effect. Each dot represents a technical replicate from an independent experiment, and each color represents an independent experiment. Each technical replicate was normalized to its independent experimental control with just J-1E6 and K562 A2/PPI cells. Statistical differences for (B) were determined by one-way ANOVA followed by Tukey's multiple comparisons test. Statistical differences for (C) were determined using a linear mixed effects model where fold change in IL-2 is predicted by the EV treatment as a linear fixed effect and the individual experiment as a random effect. ns = non-significant, * $p < 0.05$, ** $p < 0.01$, *** $p < 0.001$, **** $p < 0.0001$. Panel (A) was created using Biorender.com.

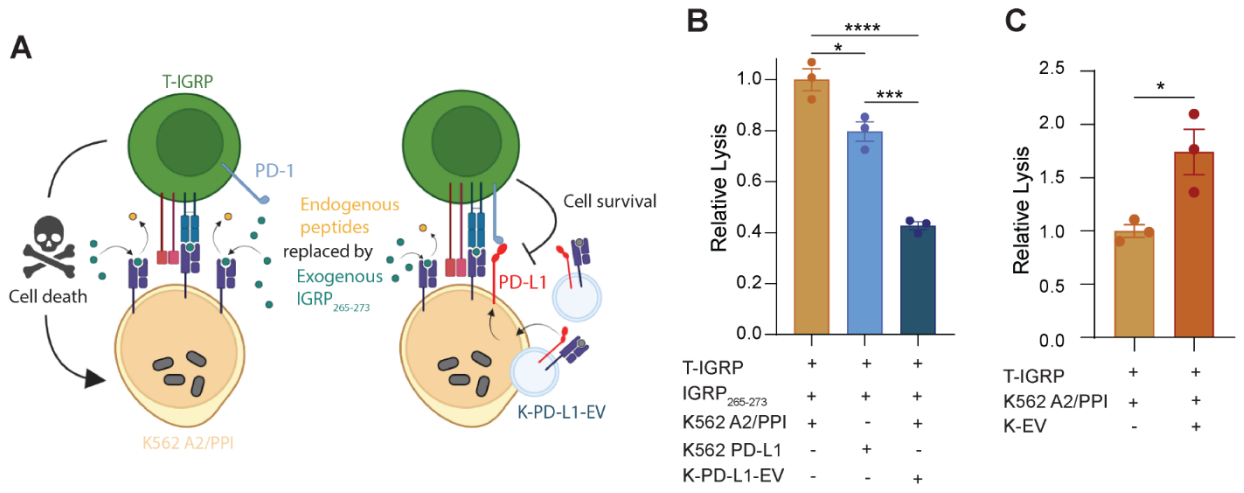

Fig. 7. EV PD-L1 reduces T cell-mediated target cell killing *in vitro*. (A) Schematic representation of T-IGRP co-cultures with K562 A2/PPI cells and K-PD-L1-EVs. (B) Specific lysis of K562 cells by T-IGRP avatars, showing a 60% reduction in specific lysis of K562 A2/PPI cells when K-PD-L1-EVs are added to co-cultures, n=3. Representative of 2 independent experiments. (C) Specific lysis of K562 A2/PPI cells by T-IGRP avatars, showing a 60-70% increase in specific lysis when K-EVs are added to co-cultures. Representative of 2 independent experiments. Statistical differences for (B) were determined by one-way ANOVA followed by Tukey's multiple comparisons test. Statistical differences for (C) were determined by unpaired, two-tailed t-test. * $p < 0.05$, *** $p < 0.001$, **** $p < 0.0001$. Panel (A) was created using Biorender.com.